Trickle-Bed Reactor Flow Simulation

David H. Anderson and Ajit V. Sapre
Mobil Research and Development Corp., Paulsboro Research Laboratory, Paulsboro, NJ 08066

A steady-state, two-dimensional model for cocurrent gas and liquid flow in a trickle-bed reactor is described. The model includes gas-liquid interaction and isothermal, incompressible flow without phase change or chemical reaction. The momentum equation proposed by Saez and Carbonell is used, along with their expressions for relative permeabilities of gas and liquid phases. Capillary pressure equations determine the difference in the pressures of flowing phases. The results of the model simulation agree with experimental data on flow distribution, liquid spreading, and phase segregation in a two-dimensional trickle bed with air-water flow in both low- and high-interaction flow regimes.

Introduction

Fixed-bed catalytic reactors with concurrent flow of gas and liquid, i.e., trickle-bed reactors, have often shown unacceptable performance levels when scaled up from laboratory to commercial reactors (e.g., Shah, 1979). Much of the performance reduction or reactor inefficiency at the large scale comes from gas/liquid flow maldistribution. However, van Klinken and van Dongen (1980) showed that very efficient gas/liquid contacting can be achieved in small-scale laboratory units due to their smaller size and use of inert fines (sand) packed into the interstices of the catalyst particles. Many previous experimental and theoretical studies have examined the effects of flow maldistribution in trickle-bed reactors because of their practical importance. The present analysis involves a multidimensional mathematical model that directly describes two-phase fluid flow in a packed bed.

Previous studies of modeling multidimensional flow in trickle beds include those of Stanek and coworkers (1981), who considered liquid distribution in a packed bed with a diffusion model. Zimmerman and Ng (1986) also developed a model for liquid distribution in a packed bed. However, each of these previous groups neglected or excluded the effects of the gas phase. Significant gas-liquid interaction occurs over the range of fluid mass fluxes used in commercial trickle-bed reactors. The present model considers the interaction of gas and liquid phases in contributing to the fluid flow behavior. Our objective is to determine the origins of maldistribution and the preferred commercial reactor design strategy for its prevention. Experimental results shown verify the model predictions.

Our model formulation for two-phase flow in porous media is similar to those widely used in petroleum reservoir simulation. The latter models are based on Darcy's law with experimentally-determined correlations of relative permeability of each phase. They are used to calculate flow rates and patterns in an oil field to aid in improving hydrocarbon recovery. A principal concern there is the time dependence of the flow. In trickle-bed reactors, we are interested primarily in flow patterns as they are affected by reactor geometry, packing properties, fluid properties, flow rates, and flow regimes.

Velocities in petroleum refining trickle beds are in the range of 0.005–0.025 m/s for liquid and 0.05–0.5 m/s for gas. These are much higher than the 5×10^{-6} m/s velocity, typically found in petroleum reservoirs. Voidage and pore/particle size in trickle beds also greatly exceed those of reservoirs. In order to apply reservoir simulation methods to the flow study in trickle beds, Saez and Carbonell (1985) developed relative permeability correlations for trickle beds based on pressure drop and liquid holdup data. In addition, Grosser et al. (1988) applied these correlations in a macroscopic flow model to describe instabilities in one-dimensional trickle beds. Our steady-state model employs the relative permeability correlations and simplified multidimensional momentum balance of Saez and Carbonell.

First, the model is developed along with appropriate boundary conditions for multidimensional flow. Then, we discuss the numerical solution method for the model. Finally, model results are shown along with experimental data for an example, two-dimensional system.

Model

Reservoir simulation includes the macroscopic (volume-averaged) models of flow in porous media that are generally

written in the Darcy's law form describing flow velocity for each phase as proportional to pressure gradient (see Aziz and Settari, 1979, for example). Effects of phase interaction are included in the relative permeability coefficients which scale the flow velocity relative to that calculated for each phase flowing individually. The describing equation for flow in a multidimensional system is (with z the coordinate oriented vertically downward)

$$\underline{u}_i = -\lambda_i(\nabla P_i - \gamma_i \nabla z) \quad i = g,1 \tag{1}$$

$\underline{u}_i$ is the superficial velocity vector of the fluid phase i, and ∇P_i is the pressure gradient in phase i. The gravity force is included in the term involving γ_i, where

$$\gamma_i = \rho_i g / g_c \quad i = g,1 \tag{1a}$$

The permeability group is defined as:

$$\lambda_i \equiv \frac{k_i k_{ri}}{\mu_i} \quad i = g,1 \tag{2}$$

In reservoir simulation, the permeability k_i depends on the physical properties of the porous medium, but not velocity or any fluid property. At the higher velocities in packed beds, pressure gradient also depends on the square of the velocity (Ergun equation, for example). This nonlinear dependence is indicated in the form of permeability used in the present model. For the liquid phase, k_L is given by:

$$k_L = 1/\left(\frac{180(1-\epsilon)^2}{d_e^2 \epsilon^3 g_c} + \frac{1.8(1-\epsilon)\rho_L |u_L|}{\mu_L d_e \epsilon^3 g_c}\right) \tag{3}$$

$|u_L|$ is the magnitude of the local velocity of liquid. For the gas-phase permeability, k_g, substitute the gas-phase properties, μ_g, ρ_g, and u_g. Equations 1-3 are derived from equations used by Saez and Carbonell, where the original equations described the pressure gradient as a function of velocities and physical properties. There, relative permeabilities were determined by evaluating the literature data of pressure drop and liquid holdup in the low-interaction, trickle-flow regime as:

$$k_{rL} = S_{Lr}^{2.43} \tag{4a}$$

$$k_{rg} = S_g^{4.8} \tag{4b}$$

S_{Lr} is the reduced saturation of the liquid phase, which subtracts out the static liquid holdup volume fraction, ϵ_L^o, which remains on the packing after stopping liquid flow.

$$S_{Lr} = (\epsilon_L - \epsilon_L^o)/(\epsilon - \epsilon_L^o) \tag{5}$$

For trickle beds, ϵ_L^o was correlated by Saez and Carbonell as:

$$\epsilon_L^o = 1/(20 + 0.9\, Eo) \tag{6a}$$

where the Eotvos number, Eo, is defined as:

$$Eo = \rho_L g d_e^2 \epsilon^2 / \sigma (1-\epsilon)^2 \tag{6b}$$

Absolute saturations of gas and liquid phases are ϵ_g/ϵ and ϵ_L/ϵ, respectively.

We will evaluate the model predictions of multidimensional flow distribution in both low- and high-interaction flow regimes. Good results were found in both flow regimes when compared with the data. This model, however, is not sufficient to describe all the details of flow behavior in the high-interaction flow regime. Grosser et al. (1988) found that inclusion of acceleration terms in the macroscopic momentum balance of Eq. 1 was necessary for determining the condition where transition occurs to an unstable, high gas-liquid interaction, pulsing-flow regime. Dankworth et al. (1990) further characterized the dynamics of pulsing flow with the same model.

The flow equations (Eqs. 1) are solved along with the steady-state equations for mass conservation for each phase, i.

$$\nabla \cdot u_i = 0 \quad i = g,1 \tag{7}$$

These equations represent incompressible flow without phase change. Substituting u_i from the flow equations produces two PDE's (partial differential equations) with unknown pressures and saturations of each phase. Auxiliary equations that are used to eliminate two of these variables include evaluation of capillary pressure (pressure difference between gas and liquid phases resulting from interfacial tension) and a balance on void volume saturation. Capillary pressure is assumed to be a function of permeability of the packing and liquid saturation of the packing voidage. Leverett (1941) proposed the following form for capillary pressure in porous media.

$$P_c = \sigma J(S_L)(\epsilon/k)^{1/2} \tag{8}$$

σ is the surface tension, k is the Darcy's law permeability, and J is a dimensionless function of only the liquid saturation. Actually, capillary pressure dependence on saturation differs between circumstances of drainage and inhibition. We neglect this hysteresis here. Grosser et al. (1988) approximated J by:

$$J = 0.48 + 0.036 \ln[(1-S_L)/S_L] \tag{9}$$

For the present model in trickle beds, capillary pressure is expected to be quite low, and we approximate this J function with a linear relationship to greatly simplify our calculations

$$J = 1 - S_L \tag{9a}$$

Void volume conservation requires

$$S_L + S_g = 1 \tag{10}$$

Substituting Eq. 1 into Eq. 7 for both gas and liquid produces two partial differential equations in terms of the pressures and saturations of each phase. But, $P_L = P_g - P_c$ by the definition of capillary pressure, and $S_L = 1 - S_g$ by Eq. 10. Therefore, Eqs. 1-10 are consolidated to produce two partial differential equations with gas-phase pressure and liquid-phase saturation as unknowns.

$$\nabla \cdot [\lambda_g(\nabla P_g - \gamma_g \nabla z)] = 0 \tag{11}$$

$$\nabla \cdot [\lambda_L(\nabla(P_g - P_c) - \gamma_L \nabla z)] = 0 \tag{12}$$

λ_i and P_c are functions of the liquid saturation.

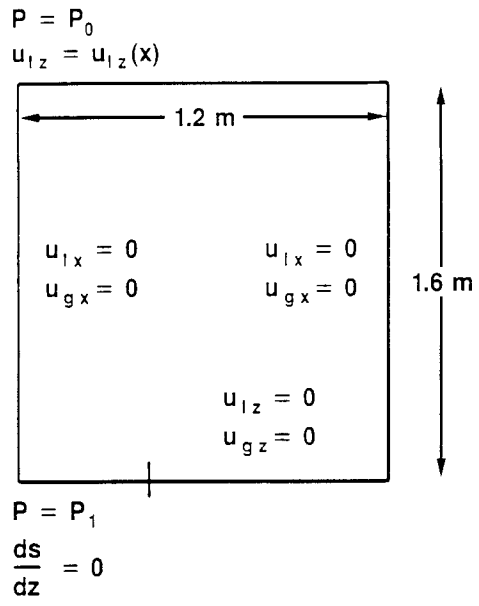

Figure 1. Two-dimensional model boundary conditions.

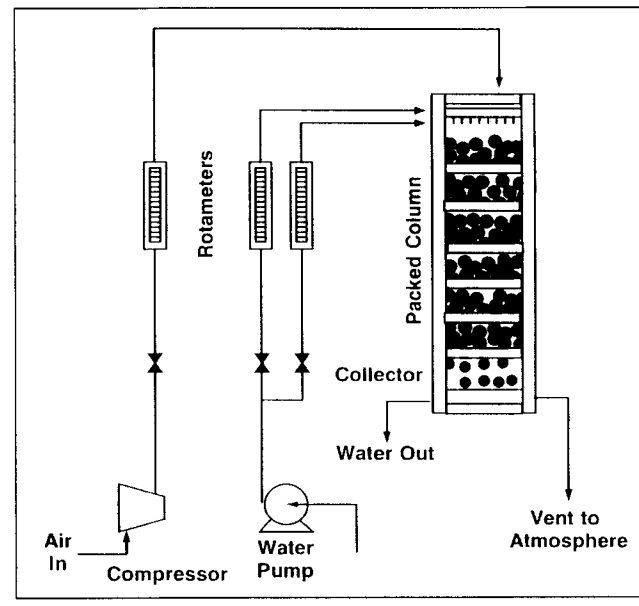

Figure 3. Laboratory trickle-bed apparatus.

Boundary Conditions

For example, the model is applied to a two-dimensional system in rectangular geometry. Flow and no-flow boundary conditions are used. Liquid velocity and gas pressure are specified at the inlet to the trickle bed. At the outlet, again gas pressure is specified, and the normal liquid saturation gradient is set to zero. Gas velocity is a result of the solution. Aziz and Settari (1979) discuss these outlet boundary conditions along with other alternatives. At the walls, there is no flow normal to the boundary. So with ∇_n the normal gradient, Eq. 1 leads to:

$$\nabla_n P_i - \gamma_i \nabla_n z = 0 \quad i = g, L \tag{13}$$

Figure 1 shows a schematic of a two-dimensional packed bed the model represents, along with the boundary conditions. In this example, the bottom is closed on the right side and open on the left.

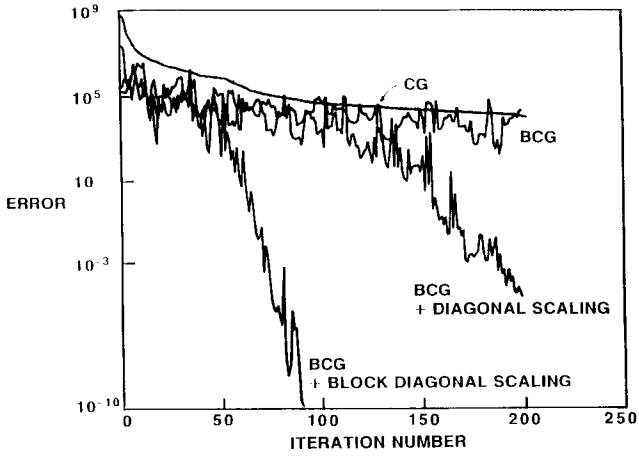

Figure 2. Performance of conjugate and bi-conjugate gradient methods.

Numerical Solution

The model equations were solved numerically in the two-dimensional, rectangular geometry shown in Figure 1 using a finite difference technique. In summary, the solution domain was discretized with uniformly spaced nodes in the vertical and horizontal dimensions. The grid size used was either 10×15 or 19×29. Discretization of PDE's converted the nonlinear PDE's to a system of nonlinear algebraic equations, with two equations at each node in the domain. These were solved using Newton's method. One major obstacle in the use of this method, though, was the need for solving large, sparse linear systems. A biconjugate gradient technique was used for this purpose to overcome constraints on computer storage and computation time.

Mikic and Morse (1985) discussed use of the biconjugate gradient (BCG) method for linear system solutions which result from solving finite-differenced PDE's describing plasma dynamics. This iterative procedure is similar to the conjugate gradient (CG) method and can be applied directly to nonsymmetric, indefinite matrix systems. Computational work for the BCG is not significantly greater than for the CG. Unlike CG, BCG does not have an error minimization property, so error will not necessarily decrease at every iteration. Mikic and Morse, however, found that when properly preconditioned, BCG rapidly converged to the solution of their linear systems.

In our evaluation of the BCG method for application to the

Table 1. Model Parameters

d_e	=	0.003 m
ϵ	=	0.39
g	=	9.8 m/s^2
g_c	=	1.0
ρ_g	=	1.44 kg/m^3
ρ_L	=	1,000.0 kg/m^3
σ	=	0.073 N/m
μ_g	=	1.5×10^{-5} Pa·s
μ_L	=	1×10^{-3} Pa·s

flow in porous media solution, effectiveness was examined relative to the CG method and the extent of preconditioning. Diagonal scaling and incomplete LU (ILU) preconditionings are used similarly as shown by Mikic and Morse. Their blockwise forms are used as well, with a 2×2 block size corresponding to the two dependent variables. Our test example is a two-dimensional system finite differenced over a 10×15 node grid, which leads to a 300-element solution vector and a 300×300 linear system matrix.

For a typical linear system in the course of our solution, Figure 2 shows convergence results when using the biconjugate gradient method with various preconditionings, as well as the use of the standard conjugate gradient method. The error shown is the sum of squared residuals of the linear solution. The CG method and unpreconditioned BCG method produce similar slow convergence results. Simple diagonal scaling preconditioning multiplies the matrix by its inverse diagonal and greatly improves convergence for the BCG method. Block diagonal scaling (BDS) involves preconditioning with the inverse block diagonal matrix, which is easily calculated. It improves convergence further. These preconditionings are easily applied, adding only sparse matrix products with a vector (Mikic and Morse, 1985). They keep the method fully vectorizable for rapid computation. Applying BDS preconditioning to the CG method did not produce significant improvements in convergence. This superior convergence of the BCG method with easily-computed preconditioning is its primary benefit.

Results vs. Experimental Data

Our two-dimensional solution geometry was chosen to match the dimensions of a 1.2-m × 1.6-m × 0.025-m-thick cold flow

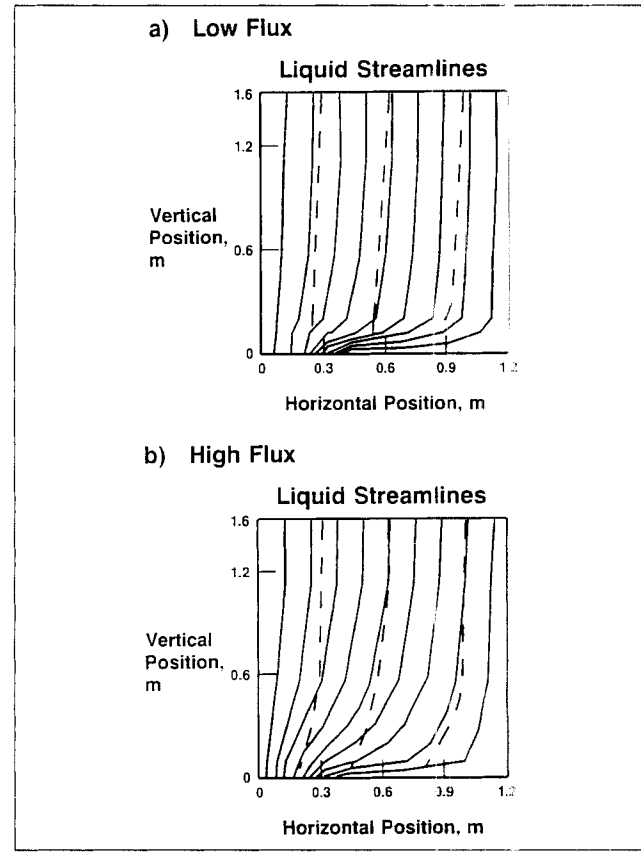

Figure 4. Liquid streamlines in trickle bed with restricted outlet.

———, model predictions; - - -, experimental results

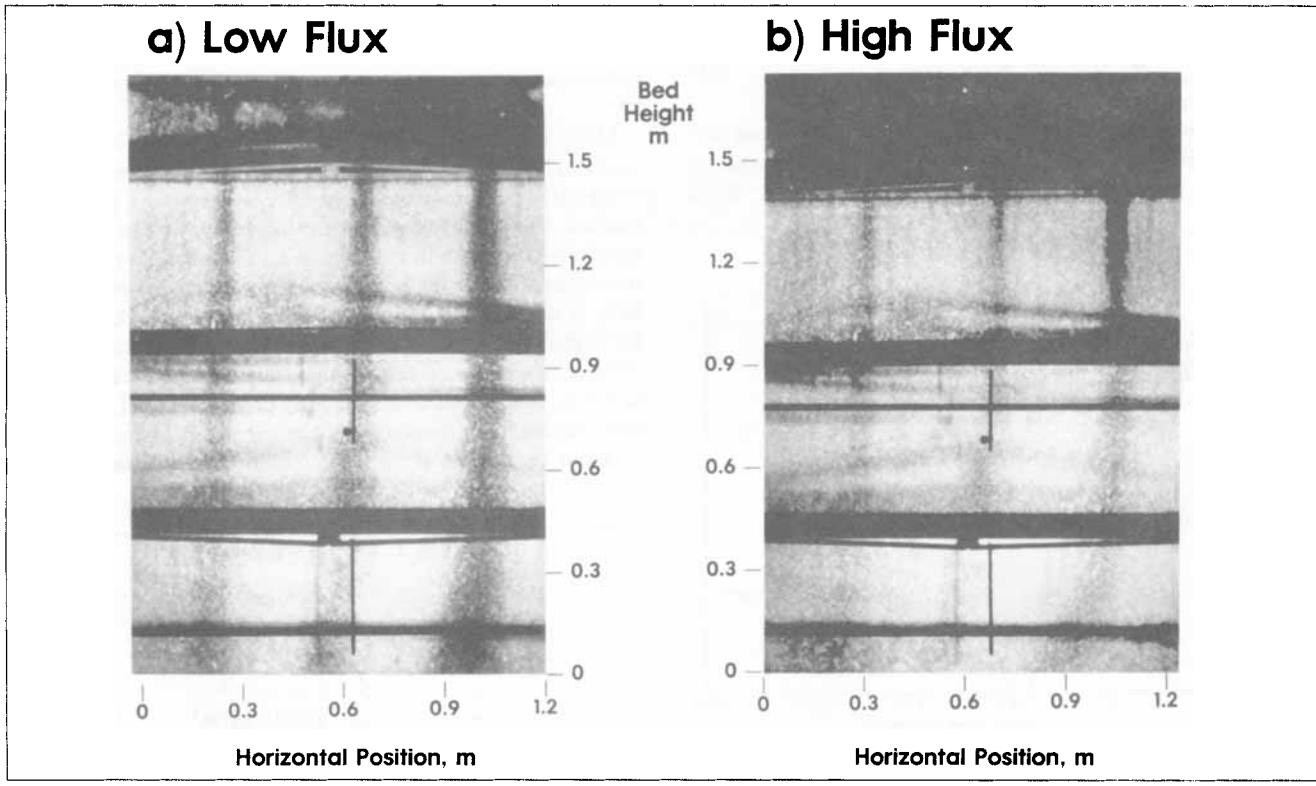

Figure 5. Cold flow experimental results.

apparatus used in our laboratory. This apparatus is similar to that described by Christensen et al. (1986). Air and water flow were used in the experiments over 0.003-m-diameter nonporous glass spheres. A schematic diagram of the apparatus is shown in Figure 3. The water was distributed over the packing at the top through 20 evenly spaced 1/4-in. (6.4-mm) tubes. Transparent walls allowed clear visualization of the flow behavior. Colored dye injected into several locations at the top indicated liquid flow paths to the outlet for comparison with model predictions. Fluid and packing physical properties of this system are shown in Table 1.

The first case, which we used to evaluate the model calculations, was the effect of a restricted outlet on the flow pattern. In this case, the bottom was open only on the left 0.4 m out of the 1.2-m width. Liquid flow was uniform over the inlet. At relatively low fluxes of 2.2 kg/m^2·s water and 0.14 kg/m^2·s air averaged over the cross-section, the liquid flow pattern remained mostly vertical and uniform until very near the bottom (Figure 4a). Pressure drop across the bed is about 4.8 kPa. However, by increasing these fluxes to 6.56 kg/m^2·s water and 0.73 kg/m^2·s air, more significant bending of the liquid streams toward the outlet was calculated (Figure 4b). Pressure drop here is about 62.1 kPa. The difference in these results occurs because gravity is more significant in influencing liquid flow in the low flux case, while the much higher pressure drop in the high flux case exhibits the greater effect of gas pressure on liquid flow. These mass fluxes represent the range of commercial trickle-bed reactor operation. Gas-liquid interaction is significant for both cases.

Figure 5 shows experimental results at the same operating conditions with the one-third outlet opening on the left side. Liquid flow was uniformly distributed through 20 equally spaced inlets at the top. The dark stripes in the figure are produced by injecting colored dye in the liquid inlets at three locations. The experimental dye paths are also indicated on Figure 4, showing that the model agrees with the data both qualitatively and quantitatively. The impact of outlet geometry in affecting upstream liquid flow distribution at high fluxes is thus demonstrated.

The low flux example was in the trickle-flow regime. However, in the high flux example, pulsing flow behavior also resulted, which is in the high interaction-flow regime. These results indicate our flow model is valid for both high- and low-interaction flow regimes for the purpose of simulating liquid flow patterns.

While liquid flow nonuniformity is greater at the higher fluxes, gas-to-liquid ratios are not constant at the lower fluxes. Figure 6 shows the flow model results that, at 0.6 m above the outlet, the gas flow profile is significantly distorted by the restricted outlet while the liquid profile is nearly uniform. For the high-flux example, both gas and liquid profiles are similarly affected. There the pressure force has become almost equally significant for the gas and liquid phases.

The second case of this study involves liquid flow introduced over only a small part of the top of the bed. For the model, the liquid flow boundary condition was set for flow over a portion of the top boundary. The water flux used was 8.4 kg/m^2·s over a single 0.076-m inlet cell width. However, the model

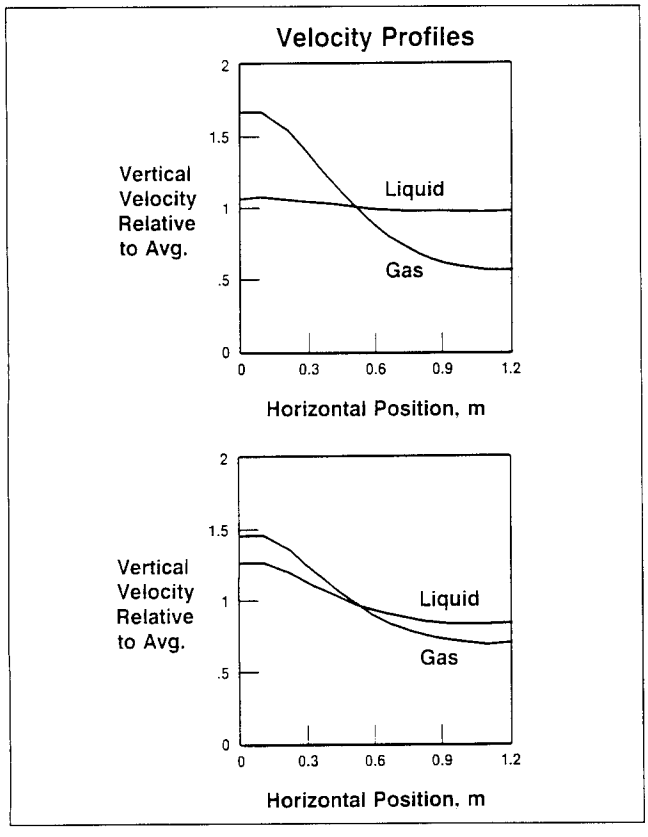

Figure 6. Velocity profiles at 0.6-m level: low flux (top); high flux (bottom).

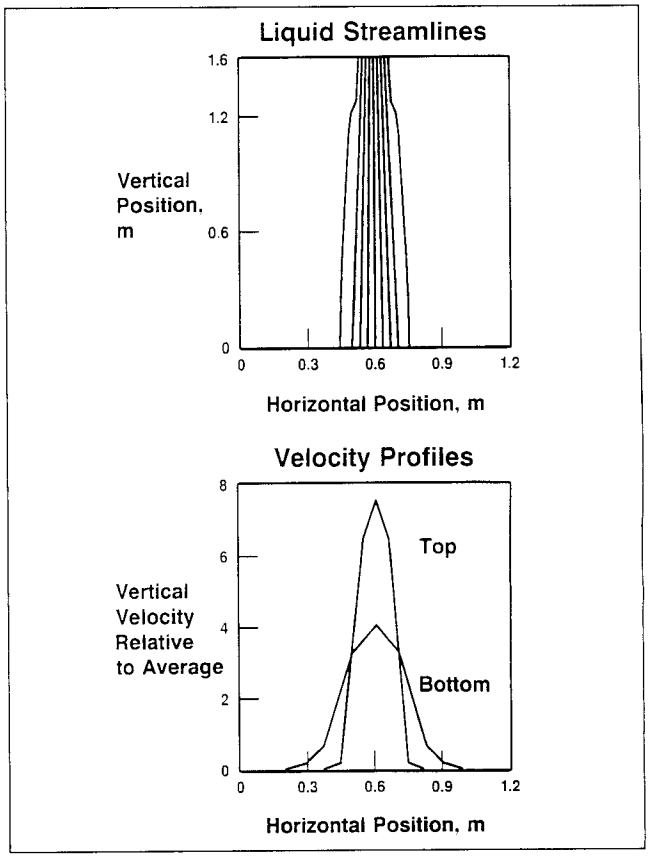

Figure 7. Narrow liquid inlet results.

calculations average this over two cells, or about 0.15 m. Average air flux was 0.73 kg/m^2·s over the bed cross-section.

Figure 7 shows liquid streamlines of the simulation: 80% of the flow is between the streamlines shown in the narrow zone beneath the inlet. We also observed in the cold flow unit only a minor degree of spreading, with the liquid flow velocity dropping off quickly outside of the region directly below the inlet. The colored tracer did not adequately reflect this behavior because of its diffusion outside the main flow region. Significant saturation gradients were present, but the lateral liquid movement was small because of the minor effect of capillary pressure. Other previous experimental results, we obtained in a 20-in. (508-mm) packed column under similar conditions, also showed only minor spreading of 1 in. (25 mm) over 10 ft (3 m) of bed depth. Therefore, significant radial mixing is not anticipated for typical trickle-bed operation based on the experimental results and our computer simulations.

Acknowledgment

We are grateful for the support and assistance of the Paulsboro Research Laboratory of Mobil Research and Development Corporation in this work.

Notation

d_e = effective particle diameter
g = gravitational constant
g_c = gravitational conversion factor
G = gas phase mass flux
J = Leverett J function
k_i = permeability of phase i
k_{ri} = relative permeability of phase i
L = liquid phase mass flux
P_i = pressure of phase i
S_i = saturation of phase i, ϵ_i/ϵ
$\underline{u}_i$ = velocity of phase i
x = horizontal coordinate
Δx = grid size
z = vertical coordinate

Greek letters

γ_i = group defined by Eq. 1a
ϵ = interparticle void fraction
ϵ_g, ϵ_L = reactor volume fractions of gas and liquid
ρ_i = density of phase i
σ = surface tension
μ_i = viscosity of phase i

Subscripts

g = gas phase
L = liquid phase

Literature Cited

Anderson, D. H., and A. V. Sapre, "Biconjugate Gradient Method of Solving Large Linear Systems in Trickle Bed Flow Simulation," *Math. Comput. Mod.*, **11**, 22 (1988).

Aziz, K., and A. Settari, *Petroleum Reservoir Simulation*, Applied Science Publishing Ltd., Essex, England (1979).

Christensen, G., S. J. McGovern, and S. Sundaresan, "Cocurrent Downflow of Air and Water in a Two-Dimensional Packed Column, *AIChE J.*, **32**, 1677 (1986).

Dankworth, D. C., I. G. Kevrekedis, and S. Sundaresan, "Dynamics of Pulsing Flow in Trickle Beds," *AIChE J.*, **36**, 605 (1990).

Grosser, K., R. G. Carbonell, and S. Sundaresan, "Onset of Pulsing in Two-Phase Cocurrent Downflow Through a Packed Bed," *AIChE J.*, **34** 1850 (1988).

Leverett, M. C., "Capillary Behavior in Porous Solids," *Trans. AIME*, **142** 152 (1941).

Mikic, Z., and E. C. Morse, "The Use of a Preconditioned Bi-Conjugate Gradient Method of Hybrid Plasma Stability Analysis," *J. Comp. Phys.*, **61**, 154 (1985).

Saez, A. E., and R. G. Carbonell, "Hydrodynamic Parameters for Gas-Liquid Concurrent Flow in Packed Beds," *AIChE J.*, **31**, 52 (1985).

Shah, Y. T., *Gas-Liquid-Solid Reactor Design*, McGraw-Hill, New York (1979).

Stanek, V., J. Hanika, V. Hlavacek, and O. Trnka, "The Effect of Liquid Flow Distribution on the Behavior of a Trickle Bed Reactor," *Chem. Eng. Sci.*, **36**, 1045 (1981).

van Klinken, J., and R. H. van Dongen, "Catalyst Dilution for Improved Performance of Laboratory Trickle-Flow Reactors," *Chem. Eng. Sci.*, **35**, 59 (1980).

Zimmerman, S. P., and K. M. Ng, "Liquid Distribution in Trickling Flow Trickle-Bed Reactors," *Chem. Eng. Sci.*, **41**, 861 (1986).

Manuscript received May 11, 1990, and revision received Jan. 8, 1991.